Drift-Induced Enhancement of Cubic Dresselhaus Spin-Orbit Interaction in a Two-Dimensional Electron Gas

Yoji Kunihashi,[1,*] Haruki Sanada,[1] Yusuke Tanaka,[1] Hideki Gotoh,[1] Koji Onomitsu,[1] Keita Nakagawara,[2] Makoto Kohda,[2] Junsaku Nitta,[2] and Tetsuomi Sogawa[1]

[1]*NTT Basic Research Laboratories, NTT Corporation, 3-1 Morinosato-Wakamiya, Atsugi, Kanagawa 243-0198, Japan*
[2]*Department of Materials Science, Tohoku University, 6-6-02 Aramaki-Aza, Aoba-ku, Sendai 980-8579, Japan*

(Received 1 March 2017; revised manuscript received 11 June 2017; published 31 October 2017)

We investigated the effect of an in-plane electric field on drifting spins in a GaAs quantum well. Kerr rotation images of the drifting spins revealed that the spin precession wavelength increases with increasing drift velocity regardless of the transport direction. A model developed for drifting spins with a heated electron distribution suggests that the in-plane electric field enhances the effective magnetic field component originating from the cubic Dresselhaus spin-orbit interaction.

DOI: 10.1103/PhysRevLett.119.187703

Electrons drifting in an electric field that breaks spatial inversion symmetry experience a momentum-dependent effective magnetic field, which enables us to manipulate their spin states without external magnetic fields. In the two-dimensional electron gas (2DEG) formed in III–V compound semiconductors, the sources of the electric fields are the crystal fields of the zinc-blende structure [1] or vertical electric fields [2] that can be tuned by using external gate voltages [3,4]. This effect, known as a spin-orbit interaction (SOI), leads to various spin-related phenomena, including the recently discovered spin Hall effect [5–7] and the persistent spin helix [8–10]. In addition to the symmetry-breaking electric fields that are converted into effective magnetic fields, most of the phenomena [5–10] and novel spintronics concepts [11–17] require lateral (or in-plane) electric fields. The application of in-plane electric fields induces drift transport and coherent spin precession simultaneously, resulting in the efficient transfer of the spins between distant places with a certain amount of spin rotation determined by the SOI. Furthermore, the strength of the in-plane electric fields will determine the spin propagation speed, which is related to the operational frequency of future spintronics devices. Thus, understanding how the in-plane electric fields affect the effective magnetic fields is important for the precise and high-speed control of drifting spins.

Recent studies have shown that the influence of in-plane electric fields on spin dynamics appears in various forms [18–23]. For example, a spin precession depending on the direction of the in-plane electric field has been used to determine the parameters for k-linear Dresselhaus and Rashba SOIs [20]. Another consequence has been observed in the transient spin grating in a drifting Fermi sea: the measurement of the phase velocity in the helical spin modes has made it possible to discuss the drifting spin dynamics [21]. A spin helix with a special symmetry is achieved under a balanced Rashba and Dresselhaus SOI condition [8–10], and this has been used to extend the length of drift spin transport [22]. All of these previous studies have focused on the role of the in-plane electric fields only as the driving force of the drifting motion. However, we expect that a further increase in the strength of the in-plane electric fields may modify the distribution of electron momentum k, giving rise to additional changes in the effective magnetic fields due to the k-cubic term of the Dresselhaus SOI.

In this Letter, we report the manifestation of a drift-induced change in an effective magnetic field, which originates from a mechanism that is different from those discussed in the previous reports mentioned above [18–23]. The Kerr rotation measurements of drifting spin profiles revealed that spin precession wavelengths increase with increasing drift velocity (v_d) regardless of the drift direction. An analysis of the data with a theoretical model revealed that these unexpected behaviors occur as a consequence of the cubic Dresselhaus SOI for electron systems being warmed by the applied in-plane electric field. Notably, this drift-induced SOI modification occurs without significant spin decoherence [24,25] and retains the symmetry useful for tailoring the balance between the Dresselhaus and Rashba SOIs [22]. Thus our finding will be of great importance for a further understanding of spin transport dynamics as well as for relevant spintronics applications using in-plane electric fields.

We first derive the spin-orbit effective magnetic fields for spins drifting steadily with momentum $\hbar\boldsymbol{k}_d$, where $\hbar$ is Planck's constant. We assume 2DEG in a (001) GaAs quantum well (QW) and define a coordinate system with base vectors $\hat{x}\|[1\bar{1}0]$, $\hat{y}\|[110]$. An electron spin with momentum $\hbar\boldsymbol{k}$ precesses around the total vector $\boldsymbol{\Omega}_{\rm tot}(\boldsymbol{k}) = \boldsymbol{\Omega}_R(\boldsymbol{k}) + \boldsymbol{\Omega}_{D1}(\boldsymbol{k}) + \boldsymbol{\Omega}_{D3}(\boldsymbol{k})$. Here, $\boldsymbol{\Omega}_R = 2\alpha(k_y, -k_x)/\hbar$ is the Rashba term [2], $\boldsymbol{\Omega}_{D1} = 2\beta_1(-k_y, -k_x)/\hbar$ is the k-linear Dresselhaus term [1], $\boldsymbol{\Omega}_{D3} = \gamma[-k_y(k_x^2 - k_y^2), k_x(k_x^2 - k_y^2)]/\hbar$ is the k-cubic Dresselhaus term, and the coefficients (α, β_1, and γ) are SOI parameters determined by the material and the QW band

profile [26]. In a small in-plane electric field, i.e., $k_d \ll k_F$, electrons fill up the Fermi circle that is shifted by $\hbar \boldsymbol{k}_d$ in the momentum space. As a starting point, we assume a degenerate limit, where only the electrons at the Fermi surface contribute to the charge and spin dynamics. When using $\boldsymbol{k}_F = k_F(\cos\theta, \sin\theta)$ and $\boldsymbol{k}_d = k_d(\cos\phi, \sin\phi)$, where θ and ϕ are the relative angles of $\boldsymbol{k}_F$ and $\boldsymbol{k}_d$ from the $[1\bar{1}0]$ direction, the vector $\boldsymbol{\Omega}_{\rm tot}$ averaged over the Fermi circle is given by $\langle \boldsymbol{\Omega}_{\rm tot} \rangle = (1/2\pi) \int_0^{2\pi} \boldsymbol{\Omega}_{\rm tot} d\theta$. The k-linear SOIs, $\boldsymbol{\Omega}_R$ and $\boldsymbol{\Omega}_{D1}$, simply lead to vectors that depend linearly on k_d,

$$\langle \boldsymbol{\Omega}_R \rangle = \frac{2\alpha}{\hbar} k_d \begin{pmatrix} \sin\phi \\ -\cos\phi \end{pmatrix}, \quad (1)$$

$$\langle \boldsymbol{\Omega}_{D1} \rangle = \frac{2\beta_1}{\hbar} k_d \begin{pmatrix} -\sin\phi \\ -\cos\phi \end{pmatrix}, \quad (2)$$

whereas $\boldsymbol{\Omega}_{D3}$ is deformed into the sum of the first- and third-order terms in k_d,

$$\langle \boldsymbol{\Omega}_{D3} \rangle = -\frac{2\beta_3}{\hbar} k_d \begin{pmatrix} -\sin\phi \\ -\cos\phi \end{pmatrix} + \frac{\gamma}{\hbar} k_d^3 \begin{pmatrix} -\sin\phi\cos 2\phi \\ \cos\phi\cos 2\phi \end{pmatrix}, \quad (3)$$

where we define $\beta_3 = \frac{1}{2}\gamma k_F^2$, and its dependence on k_F is important as regards the understanding of our experimental results, which we describe later.

In the experiment described below, we can directly observe the spatial frequency of the spin precession, $k_{\rm SO}(k_d, \phi) = v_d^{-1} |\langle \boldsymbol{\Omega}_{\rm tot}(k_d) \rangle| = m^*/\hbar k_d |\langle \boldsymbol{\Omega}_{\rm tot}(k_d) \rangle|$, as a measure of the SOI strength, where m^* is the effective electron mass. The exponents of k_d in $k_{\rm SO}(k_d, \phi)$ are reduced by 1 compared with those in $\langle \boldsymbol{\Omega}_{\rm tot}(k_d, \phi) \rangle$, so the contributions from $\langle \boldsymbol{\Omega}_R \rangle$, $\langle \boldsymbol{\Omega}_{D1} \rangle$, and the k_d-linear term of $\langle \boldsymbol{\Omega}_{D3} \rangle$ are independent of k_d, while that from the k_d-cubic term of $\langle \boldsymbol{\Omega}_{D3} \rangle$ depends quadratically on k_d.

We grew a 15-nm-thick modulation-doped GaAs-$Al_{0.3}Ga_{0.7}$ single QW on a (001) semi-insulating GaAs substrate by molecular-beam epitaxy. The QW was located 120 nm below the surface. The wafer was fabricated into a 250-μm-wide cross-shaped channel with four Ohmic contacts [Fig. 1(a)]. The channel was covered with a semitransparent Au gate electrode through which we obtain the optical signal from the QW. The spatial distribution of the drifting spins was measured by Kerr rotation microscopy with a cw Ti:sapphire laser. The photon energy of the laser was fixed at 1.529 eV, which was slightly larger than the band edge of the present QW. Spin-polarized electrons were generated with a circularly polarized pump beam and embedded in the flow of the background electrons. The spin density was detected by a linearly polarized probe beam via the Kerr rotation angle θ_K. The full widths at half maximum of the focused pump and probe lasers were 7 and 3 μm, respectively. All optical measurements were carried out at 8 K and a gate voltage of -5.0 V. We confirmed that v_d estimated with a time-resolved Kerr rotation measurement was proportional to the in-plane voltage [Fig. 1(b)]. The carrier density and mobility under this condition were estimated to be 1.2×10^{11} cm^{-2} and 7.8 m^2/Vs, respectively [27]. Under all the experimental conditions, the maximum in-plane electric field was estimated to be lower than 10 kV/m. In such moderate electric fields, the 2DEG might heat up to some extent, but the effect is not strong enough to lead to v_d saturation due to optical phonon emission, which probably influences the relevant spin decoherence mechanism [28].

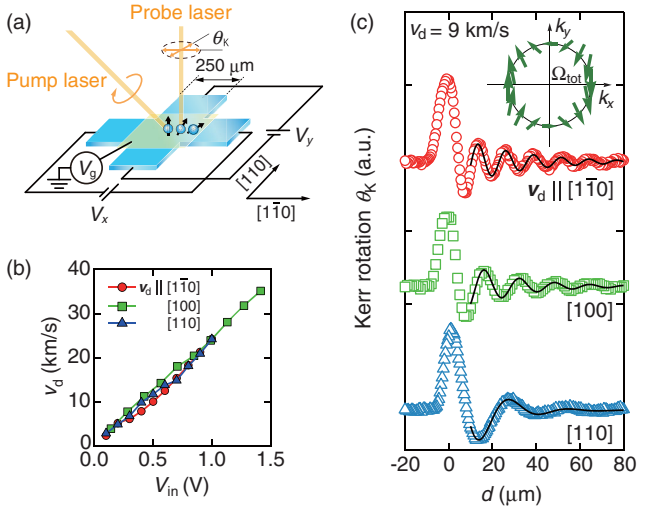

FIG. 1. (a) Schematic image of sample. (b) v_d as a function of in-plane voltage for three directions. The applied in-plane voltages (V_x, V_y) were (V_{in}, 0), (0, V_{in}), and ($V_{in}/\sqrt{2}$, $V_{in}/\sqrt{2}$) for the [1$\bar{1}$0], [110], and [100] directions. (c) Spatial distribution of drifting spins in the three directions at v_d = 10 km/s. Solid lines indicate fitted curves. Inset shows $\boldsymbol{\Omega}_{\rm tot}$ in k-space for given SOI parameters.

The drift transport of optically injected electron spins was detected as the spatially damped oscillation of θ_K as shown in Fig. 1(c), which reveals the spin dynamics of drifting electrons due to the spin-orbit effective magnetic fields. The significant dependence of the spin precession profiles on the drift direction is caused by the interplay between the Rashba and Dresselhaus SOIs [22]. To estimate the $k_{\rm SO}$ values, we fitted the experimental data for $d > 10$ μm with the function $\theta_K = A \exp(-d/l_{\rm SO}) \cos(k_{\rm SO} d)$, where d is the distance between the pump and probe beams and $l_{\rm SO}$ is the spin decay length.

The extracted $k_{\rm SO}$ values for different drift directions provide clues as regards identifying the origin of the SOIs. When v_d is sufficiently small [Fig. 1(c)], the SOI parameters, α and $\tilde{\beta} = \beta_1 - \beta_3$, can be determined by measuring $k_{\rm SO}$ for two different directions. Because $k_d \ll k_F$, we neglect the k_d-cubic term of $\langle \boldsymbol{\Omega}_{D3} \rangle$, and thus $k_{\rm SO}(\phi) = (2m^*/\hbar^2)|\sqrt{\alpha^2 + \tilde{\beta}^2 + 2\alpha\tilde{\beta}\cos(2\phi)}|$. We chose the $k_{\rm SO}$ of spins drifting in the [1$\bar{1}$0] and [110] directions with an applied in-plane voltage of 0.4 V, which corresponds to v_d = 9 km/s. The results gave us

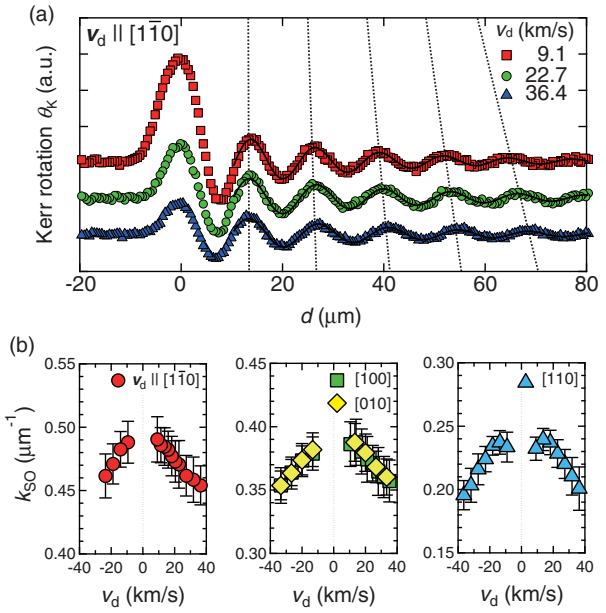

FIG. 2. (a) Spatial distribution of spins drifting in the [1$\bar{1}$0] direction at $v_d = 9.1$, 22.7, and 36.4 km/s. Solid lines are fitted to the data using the model function. Dotted lines are guides for the eye to indicate the spatial shift of the local maxima of the oscillating signals. (b) Spatial frequency of spin precession as a function of v_d for various directions. Error bars indicate a standard deviation resulting from the least-squares fit.

$k_{SO}(\phi = 0) = (2m^*/\hbar^2)|\alpha + \tilde{\beta}| = 0.49 \pm 0.02\ \mu\text{m}^{-1}$ and $k_{SO}(\phi = \pi/2) = (2m^*/\hbar^2)|\alpha - \tilde{\beta}| = 0.23 \pm 0.01\ \mu\text{m}^{-1}$. The theoretical values of α and $\tilde{\beta}$, which are calculated separately with a band profile simulation, support the idea that $\tilde{\beta} > \alpha > 0$. We thus determined the SOI parameters as $\alpha = 0.73 \pm 0.03$ and $\tilde{\beta} = 2.09 \pm 0.09$ meV Å, resulting in an anisotropic spin-orbit field in momentum space [Fig. 1(c), inset].

The data measured at higher in-plane electric fields disclose changes in the spin precession wavelengths for different v_d values. The spin profiles in Fig. 2(a) show the v_d-dependent shift of the precession phase that becomes clearer with increasing pump-probe distance. k_{SO} values extracted by fitting are plotted in Fig. 2(b) as functions of v_d. The overall trend in Fig. 2(b) is that k_{SO} decreases monotonically with an increase in v_d for all crystallographic directions, indicating that the total effective magnetic fields are weakened by applying in-plane electric fields. This behavior cannot be explained straightforwardly by the analytical expression of $\mathbf{\Omega}_{tot}(k_d)$ described in Eqs. (1)–(3). In what follows, we discuss the probable causes of this unexpected result.

The enhancement of the k_d-cubic term in $\langle \mathbf{\Omega}_{D3} \rangle$ can be ruled out as the origin of the observed v_d-induced suppression of k_{SO}. The k_d^2 ($= 4.0 \times 10^{14}$ m^{-2}) estimated from v_d at the maximum in-plane voltage employed in the experiment is still 1 order of magnitude smaller than k_F^2 ($= 7.6 \times 10^{15}$ m^{-2}), suggesting that the k_d-cubic term in $\langle \mathbf{\Omega}_{D3} \rangle$ is negligible compared with the other terms. In addition, the above theory predicts that the k_d-cubic term in $\langle \mathbf{\Omega}_{D3} \rangle$ disappears when k_d is parallel to [100] (i.e., $\phi = \pi/4$); however, the experimental data show a clear dependence on k_d even for the [100] direction.

Moreover, the phenomena cannot be explained by unintentional modifications of the k-linear SOIs ($\langle \mathbf{\Omega}_R \rangle$ and $\langle \mathbf{\Omega}_{D1} \rangle$). If the only contribution is from these k-linear terms, the spatial precession frequencies become $k_{SO}(\phi = 0) = (2m^*/\hbar)(\beta_1 + \alpha)$ and $k_{SO}(\phi = \pi/2) = (2m^*/\hbar)(\beta_1 - \alpha)$, which have no explicit k_d dependence. If we assume a monotonic change in α, which may be caused by an unintended modification of the vertical electric field, the changes in k_{SO} should have opposite signs. This does not agree with the data in Fig. 2(b). Because $\beta_1 > \alpha > 0$, k_{SO} for both drift directions may decrease if only β_1 decreases while α remains unchanged. The quantum-confined Stark effect possibly modifies $\beta_1 = \gamma \langle k_z^2 \rangle$; however, it requires large vertical electric fields that should simultaneously induce a large change in α. Thus, we can exclude the changes in α and β_1 as the cause of the v_d-dependent k_{SO}.

The remaining possibility is that β_3 in the cubic Dresselhaus SOI is enhanced by the heating of the electron system with the increasing in-plane electric field. As β_3 in Eq. (3) contains k_F, a modification of the electron distribution in a momentum space could affect the change in the precession frequency. It is natural to consider that the application of an in-plane electric field induces blurring of the Fermi surface and an increase in the average kinetic energy. The effect of electron heating appears in the shape of the photoluminescence (PL) peak assigned to the excitons formed in the QW [29]. Figure 3(a) shows PL spectra measured for various drift velocities by using an excitation laser whose wavelength was 760 nm. The two PL peaks centered at 1.527 and 1.534 eV are due to the recombination of an electron with a heavy hole and an electron with a light hole, respectively. As shown in Fig. 3(a), the high-energy tail of the PL peak becomes pronounced as v_d increases. By comparing the slopes of these tails with those measured without in-plane electric fields at different lattice temperatures, we roughly estimate the electron temperature T_e to reach 46 K at $v_d = 36$ km/s [27].

To understand how the electron heating influences the effective magnetic field, we simply extend the above model for the degenerate 2DEG to the nondegenerate case by using the Fermi-Dirac function: $f(\varepsilon) = \{1 + \exp[(\varepsilon - \mu)/k_B T_e]\}^{-1}$, where T_e is included as the system temperature, $\varepsilon = (\hbar^2/2m^*)(k_x^2 + k_y^2)$ is the kinetic energy of the two-dimensional electrons, μ is the chemical potential, and k_B is the Boltzmann constant [Fig. 3(b)]. The effective magnetic field is averaged over all the constituent electrons, and this can be approximated by the integration of $\langle \mathbf{\Omega}_{tot}(\varepsilon) \rangle$ multiplied by the weighting

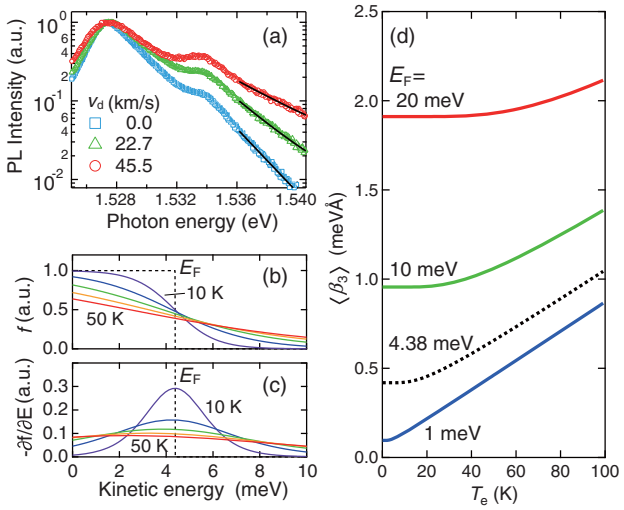

FIG. 3. (a) Photoluminescence spectra with and without applied in-plane voltage. Solid lines indicate the fitting results with an exponential function. (b),(c) Fermi-Dirac distribution functions (b) and its first derivative with respect to energy (c) plotted as functions of kinetic energy for various electron temperatures. (d) Electron temperature dependence of cubic Dresselhaus parameter β_3 calculated with $\gamma = 11$ eV Å^3 for various Fermi energies.

function $w(\varepsilon) \propto -\partial f/\partial\varepsilon$, where k_F in Eq. (3) is replaced by $\sqrt{2m^*\varepsilon}/\hbar$. The profile of $w(\varepsilon)$ is plotted in Fig. 3(c). At the degenerate limit ($T_e = 0$ K), $w(\varepsilon)$ is a δ function at $\varepsilon = E_F = \pi\hbar^2 n_s/m^*$, and a small increase in T_e ($k_B T_e \ll E_F$) makes the $w(\varepsilon)$ peak wider, but it is still symmetric at $\varepsilon = E_F$. As T_e increases further, the center of the peak ($\varepsilon = \mu$) starts to shift from E_F to a lower energy because the total electron density n_s has to be maintained while the broadened distribution is cut off at $\varepsilon = 0$. This behavior of μ versus T_e results in an increase in the average kinetic energy $\langle\varepsilon\rangle = E_F/[1 - \exp(-E_F/k_B T_e)]$, which determines the effective magnetic fields experienced by the heated 2D electron system.

As already mentioned, the only $\langle\mathbf{\Omega}\rangle$ component that depends on k_F is the k_d-linear term of the cubic Dresselhaus SOI [Eq. (3)], in which the coefficient $\beta_3 = \frac{1}{2}\gamma k_F^2 = \gamma m^*\varepsilon/\hbar^2$ becomes linear in ε. Thus, we obtain

$$\langle\beta_3\rangle = \frac{\gamma m^*}{\hbar^2}\frac{E_F}{1 - \exp(-E_F/k_B T_e)}. \tag{4}$$

We plot $\langle\beta_3\rangle$ calculated for various Fermi energies in Fig. 3(d). Here we used $\gamma = 11$ eV Å^3 [30]. To explain their behavior, we separate T_e into two regions: $k_B T_e \ll E_F$ and $k_B T_e \gtrsim E_F$. In the former, $\langle\beta_3\rangle \approx \gamma m^* E_F/\hbar^2$ stays constant and is not influenced by the blurring of the Fermi surface. In the latter, as T_e increases, $\langle\beta_3\rangle$ increases and approaches the linear function $\langle\beta_3\rangle \approx (\gamma m^*/\hbar^2)(\frac{1}{2}E_F + k_B T_e)$. Note that the boundary between these two T_e regions is characterized by $E_F \propto n_s$, suggesting that, for a larger n_s, the $\langle\beta_3\rangle$ enhancement occurs at a higher T_e. In other words, this effect will be pronounced in systems with a lower carrier density.

This model indicates that the effect of $\langle\beta_3\rangle$ enhancement appears as a decrease in k_{SO} for all drift directions. Because the $\langle\Omega\rangle$ component described with $\langle\beta_3\rangle$ has the same angle dependence as that with β_1, an increase in $\langle\beta_3\rangle$ reduces $\tilde{\beta} = \beta_1 - \langle\beta_3\rangle$. The drift direction ($\phi$) dependence of $\langle\Omega\rangle$ shown in Eqs. (1)–(3) gives us $k_{SO}(\phi = 0) \propto \tilde{\beta} + \alpha$, $k_{SO}(\phi = \pi/4) \propto \sqrt{\tilde{\beta}^2 + \alpha^2}/2$, and $k_{SO}(\phi = \pi/2) \propto \tilde{\beta} - \alpha$. By considering these angle dependences with the relation $\tilde{\beta} > \alpha > 0$, it is clear that k_{SO} for all the drift directions decreases monotonically with increasing $\langle\beta_3\rangle$. The plots of k_{SO} versus T_e shown in Fig. 4 compare the model with the experiment. The decreases in k_{SO} and their drift-direction dependence in the experimental data both agree well with the calculation. We infer that the low carrier density ($n_s = 1.2 \times 10^{11}$ cm^{-2}) likely contributed to the enhancement of $\langle\beta_3\rangle$ in an electric field of around 10 kV/m, in agreement with the density-dependent characteristics revealed by the model. The same characteristics also could be the reason why the v_d dependence of the k_{SO} was not observed in the previous experiment [23], where the drifting spins with higher carrier density ($n_s = 5 \times 10^{11}$ cm^{-2}) were investigated.

In summary, we have investigated the effect of an in-plane electric field on drifting spins in a GaAs QW. The experimentally obtained spin precession wavelengths of drifting electrons were unexpectedly elongated by increasing the in-plane electric field regardless of the drift direction. The model developed for the drifting spins in the heated electron system suggested that the in-plane electric field could enhance the effective magnetic field component originating from the k-cubic term of the Dresselhaus SOI. In general, an increase in electron temperature is unwanted in many semiconductor experiments since it may complicate most phenomena in the electron system. However, the situation is unavoidable when we require the highest electric fields possible for the efficient and rapid transport of electron spins. Our results show that the effect of electron heating is the correction of

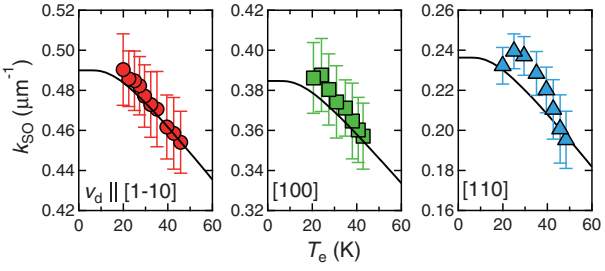

FIG. 4. Electron temperature dependence of spatial frequency of spin precession for drifting spins in the [1$\bar{1}$0], [100], and [110] directions. Solid lines indicate values calculated with Eq. (4).

the k_d-linear term of the effective magnetic field rather than as spin decoherence due to the D'yakonov-Perel' mechanism with the enhancement of the cubic Dresselhaus SOI [24,28]. Because this simple modification retains the symmetry of the k-linear Dresselhaus and Rashba SOIs, it is still possible for us to tailor a modified total effective magnetic field by adjusting the external gate bias voltage or designing the device structure. Thus, our finding will be beneficial for a further understanding of SOI-related phenomena as well as for spintronics applications using spin transport with electric fields in semiconductors.

We thank H. Irie and K. Sasaki for useful discussions. This work was supported by Japan Society for the Promotion of Science (JSPS) KAKENHI Grants No. JP15H05699 and No. JP16H03821.

*kunihashi.y@lab.ntt.co.jp

[1] G. Dresselhaus, Phys. Rev. **100**, 580 (1955).
[2] Y. Bychkov and E. I. Rashba, P. Zh. Eksp. Teor. Fiz. **39**, 66 (1984) [JETP Lett. **39**, 78 (1984)].
[3] J. Nitta, T. Akazaki, H. Takayanagi, and T. Enoki, Phys. Rev. Lett. **78**, 1335 (1997).
[4] A. Balocchi, Q. H. Duong, P. Renucci, B. L. Liu, C. Fontaine, T. Amand, D. Lagarde, and X. Marie, Phys. Rev. Lett. **107**, 136604 (2011).
[5] J. E. Hirsch, Phys. Rev. Lett. **83**, 1834 (1999).
[6] S. Zhang, Phys. Rev. Lett. **85**, 393 (2000).
[7] J. Wunderlich, B. Kaestner, J. Sinova, and T. Jungwirth, Phys. Rev. Lett. **94**, 047204 (2005).
[8] J. Schliemann and D. Loss, Phys. Rev. B **68**, 165311 (2003).
[9] B. A. Bernevig, J. Orenstein, and S.-C. Zhang, Phys. Rev. Lett. **97**, 236601 (2006).
[10] J. D. Koralek, C. P. Weber, J. Orenstein, B. A. Bernevig, S.-C. Zhang, S. Mack, and D. D. Awschalom, Nature (London) **458**, 610 (2009).
[11] S. Datta and B. Das, Appl. Phys. Lett. **56**, 665 (1990).
[12] J. Wunderich, B. G. Park, A. C. Irvine, L. P. Zârbo, E. Rozkotová, P. Nemec, V. Novák, J. Sinova, and T. Jungwirth, Science **330**, 1801 (2010).
[13] X. Cartoxiá, D. Z.-Y. Ting, and Y.-C. Chang, Appl. Phys. Lett. **83**, 1462 (2003).
[14] J. Schliemann, J. C. Egues, and D. Loss, Phys. Rev. Lett. **90**, 146801 (2003).
[15] Y. Kunihashi, M. Kohda, H. Sanada, H. Gotoh, T. Sogawa, and J. Nitta, Appl. Phys. Lett. **100**, 113502 (2012).
[16] S. A. Wolf, D. D. Awschalom, R. A. Buhrman, J. M. Daughton, S. von Molnár, M. L. Roukes, A. Y. Chtchelkanva, and D. M. Treger, Science **294**, 1488 (2001).
[17] M. Kohda, S. Nakamura, Y. Nishihara, K. Kobayashi, T. Ono, J. Ohe, Y. Tokura, T. Mineno, and J. Nitta, Nat. Commun. **3**, 1082 (2012).
[18] J. M. Kikkawa and D. D. Awschalom, Nature (London) **397**, 139 (1999).
[19] Y. Kato, R. C. Myers, A. C. Gossard, and D. D. Awschalom, Nature (London) **427**, 50 (2004).
[20] L. Meier, G. Salis, I. Shorubalko, S. S. E. Gini, and K. Ensslin, Nat. Phys. **3**, 650 (2007).
[21] L. Yang, J. D. Koralek, J. Orenstein, D. R. Tibbetts, J. L. Reno, and M. P. Lilly, Nat. Phys. **8**, 153 (2012).
[22] Y. Kunihashi, H. Sanada, H. Gotoh, K. Onomitsu, M. Kohda, J. Nitta, and T. Sogawa, Nat. Commun. **7**, 10722 (2016).
[23] P. Altmann, F. G. G. Hernandez, G. J. Ferreira, M. Kohda, C. Reichl, W. Wegscheider, and G. Salis, Phys. Rev. Lett. **116**, 196802 (2016).
[24] H. Sanada, I. Arata, Y. Ohno, Z. Chen, K. Kayanuma, Y. Oka, F. Matsukura, and H. Ohno, Appl. Phys. Lett. **81**, 2788 (2002).
[25] Y. Sato, Y. Takahashi, Y. Kawamura, and H. Kawaguchi, Jpn. J. Appl. Phys. **43**, L230 (2004).
[26] R. Winkler, *Spin-Orbit Coupling Effects in Two-Dimensional Electron and Hole Systems* (Springer, New York, 2003).
[27] See Supplemental Material at http://link.aps.org/supplemental/10.1103/PhysRevLett.119.187703 for details on the estimations of the carrier density, mobility, and election temperature.
[28] M. Q. Weng, M. W. Wu, and L. Jiang, Phys. Rev. B **69**, 245320 (2004).
[29] J. Shah, Solid State Electron. **21**, 43 (1978).
[30] M. P. Walser, U. Siegenthaler, V. Lechner, D. Schuh, S. D. Ganichev, W. Wegscheider, and G. Salis, Phys. Rev. B **86**, 195309 (2012).